

Adaptive transmission for radar arrays using Weiss-Weinstein bounds

Christian Greiff, David Mateos-Núñez, María A. González-Huici, Stefan Brüggewirth

This paper is a preprint of a paper accepted by IET Radar, Sonar & Navigation and is subject to Institution of Engineering and Technology Copyright. When the final version is published, the copy of record will be available at the IET Digital Library

Abstract—We present an algorithm for adaptive selection of pulse repetition frequency or antenna activations for Doppler and DoA estimation. The adaptation is performed sequentially using a Bayesian filter, responsible for updating the belief on parameters, and a controller, responsible for selecting transmission variables for the next measurement by optimizing a prediction of the estimation error. This selection optimizes the Weiss-Weinstein bound for a multi-dimensional frequency estimation model based on array measurements of a narrow-band far-field source. A particle filter implements the update of the posterior distribution after each new measurement is taken, and this posterior is further approximated by a Gaussian or a uniform distribution for which computationally fast expressions of the Weiss-Weinstein bound are analytically derived. We characterize the controller's optimal choices in terms of SNR and variance of the current belief, discussing their properties in terms of the ambiguity function and comparing them with optimal choices of other Weiss-Weinstein bound constructions in the literature. The resulting algorithms are analyzed in simulations where we showcase a practically feasible real-time evaluation based on look-up tables or small neural networks trained off-line.

I. INTRODUCTION

Software-defined radar systems offer degrees of freedom such as waveform diversity, beam-steering, or antenna selection. The concept of Cognitive Radar [1] describes a dynamic systems approach for the control of these degrees of freedom in a real-time, closed-loop fashion, motivating research on waveform design [2]–[4], matched illumination [5], [6], radar resource management [7], [8], or spectral coexistence [9], [10]. Application areas include multi-functional active electronically scanned array (AESA) systems in airborne or maritime scenarios [11], [12], automotive multiple-input multiple-output (MIMO)-radars [13]–[15] or distributed sensor networks [16].

The *perception-action* cycle [17], [18] describes a sequential process of extracting information from a scene and using that knowledge for adapting the transmission and processing of subsequent measurements. These are tasks of estimation and control that can be formulated in a Bayesian estimation framework [19], [1]. Sequential estimation is performed by updating a belief distribution over the parameter of interest according to motion and measurement models, which is suitable for tracking and Track-Before-Detect approaches. Practical implementations such as Particle Filters [20] or Cubature Kalman Filters [1] can handle nonlinear models crucial for radar systems. On the control side, the estimation performance can be predicted and optimized using Bayesian

bounds [19] that provide a lower bound on the expectation over the current belief of the covariance matrix of the error of any estimator. Classical examples include the Bayesian Cramer-Rao bound (BCRB), and other members of the family of Weiss-Weinstein bounds (WWB) [21], [22], including the Bobrovsky-Zakai bound (BZB). The latter, together with the Ziv-Zakai bound (ZZB) [23], take into account estimation errors in nonlinear estimation problems that occur below a certain signal-to-noise ratio (SNR) due to sidelobes in the ambiguity function [24]. These are underestimated by the Cramér-Rao bound (CRB), which is related to the mainlobe-width and therefore measures the accuracy and resolution limit when the SNR is large. Instances of such nonlinear estimation problems include frequency estimation in radar systems such as the estimation of Doppler frequency and direction of arrival (DoA). These scenarios have been the context for adaptive strategies for the selection of pulse repetition frequency [25] using the BCRB, and for antenna selection using the BZB [14], [15] and Weiss-Weinstein bound (WWB) [26].

The optimization metrics prescribed by the WWB are themselves an optimization over so-called test points of an expression that contains integrals of the measurement and prior distributions. These probability models affect the characterization of optimal sensing parameters, and also the existence of analytical expressions for the integrals. In the context of sequential estimation of a dynamic Markovian parameter, these metrics can be constructed to bound the Bayesian mean squared error (BMSE) given all previous measurements. In this case, the motion and measurement updates can be embedded in a sequential computation of the WWB under an ample class of dynamics [27], resulting in explicit formulas for some families of prior and measurement distributions [28]. Alternatively, the works [13], [14], [29] show that under exact posteriors, the Bayesian bound becomes too a conditional bound given previous measurements, and suggest approximating these posteriors with a particle filter or the Metropolis-Hastings algorithm. In this work we use a particle filter to update the posterior, that is further approximated by a combination of Gaussian and uniform distributions for the selection of sensing parameters using the WWB. For this purpose and those priors, we have derived the WWB for frequency estimation using array measurement models for a single source with known SNR but random initial phase, with a rigorous derivation of test-point domains. This model can be particularized to azimuth and elevation estimation, azimuth and Doppler estimation in time-division multiplexing (TDM) MIMO. Modeling-wise, in the case of DoA or Doppler estimation, we characterize the

WWB-based optimal selection of a scaling parameter that models the carrier frequency or the pulse repetition interval (PRI), in terms of the field of view (FoV) or variance of the prior density, and compare the benefits of the proposed model with alternative WWB constructions called *conditional*, which we refer to as *known-phase*, and *unconditional* signal models [30], demonstrating the influence of modeling the initial phase as random while regarding the SNR as deterministic and known. Computationally, this formulation has the advantage of fast, vectorized evaluation over test-points thanks to explicit formulas without needing to evaluate the inverse of a matrix. We then show in simulations the closed-loop performance of the particle filter combined with the above criteria using feedback on the variance of the posterior for adaptation of pulse repetition frequency (PRF) or array scaling, and for antenna selection.

Organization: The paper is organized as follows: Section II describes the adaptive sensing algorithm for sequential Bayesian estimation. Section III presents a derivation of the WWB for general array processing tasks for a single source of known SNR under a spatio-temporal sampling scheme with a random initial phase associated to the coherent processing interval. Section IV includes an analysis of the controller choices for several WWB models and analyzes the consequences of assuming knowledge of the initial phase or lack thereof. Section V applies the general framework to the problem of adaptive PRF or array scaling for Doppler or DoA estimation, and to the problem of channel selection for DoA estimation. The resulting adaptive policies are compared in simulations, exemplifying the practical implementation of our strategies with the use of look-up tables and neural nets. Section VI discusses our conclusions and ideas for future work, and we include Appendices with auxiliary results.

Notational conventions: \mathbb{R}^N and \mathbb{C}^N denote the N -dimensional real and complex vector spaces, respectively. The real part of a complex number $z \in \mathbb{C}$ is $\text{Re}\{z\}$, while $|z|$ stands for the absolute value. Likewise, the Euclidean volume for sets $\Theta \subset \mathbb{R}^q$ is denoted by $|\Theta| = \int \chi_\Theta(\boldsymbol{\theta}) d\boldsymbol{\theta}$, where χ_Θ is the indicator function. For a symmetric real or Hermitian complex matrix \mathbf{A} , the induced norm is $\|\mathbf{x}\|_{\mathbf{A}} := \sqrt{\mathbf{x}^H \mathbf{A} \mathbf{x}}$ where \mathbf{x}^H is the conjugated transpose of vector \mathbf{x} . The weighted trace is defined as $\text{trace}_\rho(\mathbf{A}) := \sum_i \rho_i A_{ii}$. We denote by $\mathbf{1}_N \in \mathbb{R}^N$ the vector of ones and $\mathbf{I}_N \in \mathbb{R}^{N \times N}$ the identity matrix. For functions, $p, f : \mathbb{R}^q \rightarrow \mathbb{R}$, we define the expectation of f with respect to the density p as $\mathbb{E}_{p(\boldsymbol{\theta})}[f] = \int f(\boldsymbol{\theta}) p(\boldsymbol{\theta}) d\boldsymbol{\theta}$. Bracketed integer superscripts serve as abbreviation for a collection of variables, e.g. $\mathbf{x}^{(k)} = \{\mathbf{x}^1, \dots, \mathbf{x}^k\}$.

We adhere to the convention that lower case letters denote scalars (e.g. $\gamma \in \mathbb{R}$), lower case boldface letter denote vectors (e.g. $\mathbf{d} \in \mathbb{R}^N$) and upper case boldface letters denote matrices (e.g. $\mathbf{H} \in \mathbb{R}^{q \times M}$). We frequently use a Matlab inspired notation for vector evaluations of a scalar function, e.g. for a vector $\mathbf{d} = (d_n)_{n=1}^N \in \mathbb{R}^N$, the expression $e^{i\mathbf{d}} = (e^{id_n})_{n=1}^N \in \mathbb{C}^N$ also denotes a vector.

II. BAYESIAN ADAPTIVE SENSING FOR SEQUENTIAL ESTIMATION

Here we describe a framework for sequential adaptive sensing using as feedback a belief distribution of the parameter of interest. The control system comprises a *processor*, which uses a Bayesian filter to incorporate information from measurements about a parameter of interest into the belief distribution, and a *controller*, which is a rule for selecting the transmission variables for the next measurement using feedback on the current knowledge. Next we describe the processor and the controller.

A. Processor

The processor is in charge of incorporating information from the latest measurement into the belief distribution of the parameter of interest. Consider a parameter vector that at time k is modeled by the random vector $\boldsymbol{\theta}_k \in \mathbb{R}^N$. To relate the measurement \mathbf{x}_k at step k with the parameter $\boldsymbol{\theta}_k$, we need a measurement model, $p(\mathbf{x}_k | \boldsymbol{\theta}_k, \mathbf{g}_k)$, that depends on the sensing parameters \mathbf{g}_k used in that measurement. In Section III, we substantiate this model focusing on multidimensional frequency estimation of a single complex sinusoid with additive Gaussian white noise where the sensing parameters are sampling schemes in time and space. We keep this section general for suitable distributions $p(\mathbf{x}_k | \boldsymbol{\theta}_k, \mathbf{g}_k)$.

To model the evolution between measurement steps of the parameter being estimated, we assume a Markovian *transition* (or state evolution) model of the form $p(\boldsymbol{\theta}_k | \boldsymbol{\theta}_{k-1}, \mathbf{g}_k)$. Note that in general there can be a dependence on the sensing parameter, e.g., if the latter specifies the time of the measurement at step k . This transition probability is assumed known.

A Bayesian filter proceeds in two steps: the motion update (or prediction) and the measurement update (or filtering). The initial belief distribution for the parameter, denoted by $p(\boldsymbol{\theta}_0) = p_0(\boldsymbol{\theta}_0)$ is a modeling choice.

Motion update: The motion update predicts the *state* of the parameter at the time of the next measurement using the model for state evolution. Suppose that after measurement step $k-1$, we have a belief given by $p_{k-1}^+(\boldsymbol{\theta}_{k-1})$. Then the motion update of the belief distribution is given by the Chapman-Kolmogorov equation [20],

$$p_k^-(\boldsymbol{\theta}_k) := \int p(\boldsymbol{\theta}_k | \boldsymbol{\theta}_{k-1}, \mathbf{g}_k) p_{k-1}^+(\boldsymbol{\theta}_{k-1}) d\boldsymbol{\theta}_{k-1}. \quad (1)$$

This probability is employed as predicted *prior* belief at step k .

Measurement update: The measurement update filters the prediction using the likelihood of the measurement,

$$p_k^+(\boldsymbol{\theta}_k) := c p(\mathbf{x}_k | \boldsymbol{\theta}_k, \mathbf{g}_k) p_k^-(\boldsymbol{\theta}_k) \quad (2)$$

with c chosen so that p_k^+ is a probability density over values of $\boldsymbol{\theta}_k$, and $p_0^+(\boldsymbol{\theta}_0) := p_0(\boldsymbol{\theta}_0)$. The recurrences (1) and (2) have properties that can depend on the policy for sensing parameters at the Controller.

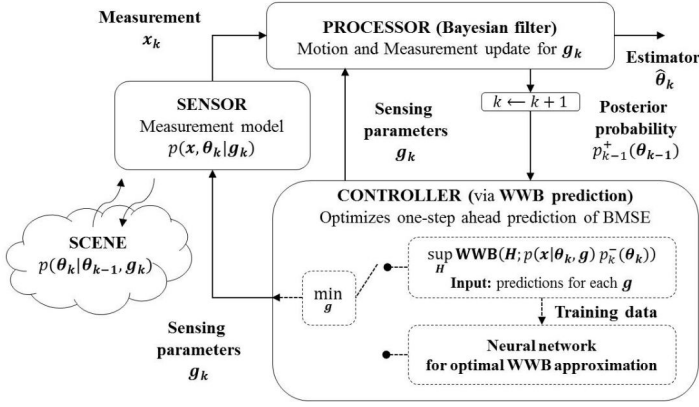


Fig. 1. Diagram of adaptive sensing based on the WWB. This Bayesian framework is analogous to the ones in [18], [26], where we consider in this work the optional choice of training a neural network for WWB ranking of candidate sensing parameters.

B. Controller

The controller is in charge of selecting sensing parameters for the next measurement using as input the current belief distribution. That is, at step k it takes as input the posterior of the last step $p_{k-1}^+(\theta_{k-1})$ before the motion update, or approximation thereof, and returns g_k . Any criterion to make this selection should employ the state evolution model $p(\theta_k | \theta_{k-1}, g_k)$ and the observation model according to candidate sensing parameters $p(x_k | \theta_k, g_k)$. The criterion used in this paper is a tight lower bound on the BMSE.

For the data model $p(x, \theta)$, the *Bayesian Mean Squared Error* (BMSE) of an estimator $\hat{\theta} \equiv \hat{\theta}(x)$ of θ is defined as the Bayesian covariance matrix of the error $e := \hat{\theta}(x) - \theta$, i.e.,

$$\text{BMSE}(\hat{\theta}; p(x, \theta)) := \mathbb{E}_{p(x, \theta)} [(\hat{\theta}(x) - \theta)(\hat{\theta}(x) - \theta)^T]. \quad (3)$$

The BMSE in (3) can be used as optimization metric for adaptive sensing [31], but is expensive to compute because it involves Monte Carlo integrals over the parameter space and over realizations of the observation. Instead, we follow the common practice of replacing the BMSE by one of its lower bounds, e.g. the *Weiss-Weinstein bound* (WWB). The WWB provides a lower bound on the BMSE of any estimator and thus gives an indication of the achievable estimation performance. Formally, the bound is obtained from a covariance inequality in the sense of the Loewner order on positive semi-definite matrices [19, p. 333] as

$$\text{WWB}(H; p(x, \theta)) \preceq \text{BMSE}(\hat{\theta}; p(x, \theta)), \quad (4)$$

where $\text{WWB}(H; p(x, \theta)) \in \mathbb{R}^{q \times q}$ is a member of the family of WWBs parametrized by the *test point matrix* H for a data model $p(x, \theta)$ as described in the Appendix A.

Depending on the estimation task, we are interested in the contribution to the BMSE of a subset of coordinates, and thus we define the following objective function for candidate sensing parameters,

$$\mathcal{C}_k(g) := \sup_H \text{trace}_\rho(\text{WWB}(H; p(x_k | \theta_k, g) p_k^-(\theta_k))), \quad (5)$$

where the predicted prior $p_k^-(\theta_k) \equiv p_k^-(\theta_k; g)$ depends on g and is obtained from the input $p_{k-1}^+(\theta_{k-1})$ through the motion update (1). The weighting vector $\rho \in \mathbb{R}_{\geq 0}^q$ can be used to balance units or weight the components of θ . Optimization over test points H is performed to obtain the tightest bound within the parametric family of bounds. The sensing parameters are then found as

$$g_k = \arg \min_g \mathcal{C}_k(g). \quad (6)$$

This selection requires a double optimization procedure, first over test point matrix H , to evaluate the prediction of the BMSE, and then over sensing parameters. The former is non-convex and we use a global optimization algorithm (e.g. simulated annealing [32]). A visualization of the closed-loop between the processor and the controller is depicted in Fig. 1. Algorithm 1 summarizes the steps.

Algorithm 1 (Adaptive selection of sensing parameters).

Input: Initial belief distribution $p_0^+(\theta)$; Measurement likelihood model $p(x | \theta, g)$; State evolution model $p(\theta_k | \theta_{k-1})$

Output: Belief distribution $p_k^+(\theta_k | g_k)$

Procedure: Set $k = 1$.

1. Motion update of belief distribution via (1) to obtain $p_k^-(\theta_k)$
2. The controller finds "optimal" sensing parameters g_k by minimizing the cost function $g_k = \arg \min_g \mathcal{C}_k(g)$
3. Measurement is performed, yielding observation x_k
4. The processor performs the measurement update of belief distribution via (2) to obtain the posterior $p_k^+(\theta_k)$
5. Start next cycle with $p_k^+(\theta_k)$ as new initial belief by increasing $k \leftarrow k + 1$ and repeating from step 1

Remark 1 (Dependence of motion model on sensing parameter). Note that if the motion update depends on the sensing parameter (e.g., if it refers to the time of measurement), then the controller has to perform the motion update in (1) for each evaluation of the cost function $\mathcal{C}_k(g)$. For the special case of a g -independent state evolution model, the motion update in (1) needs to be performed only once before passing the resulting prediction to the controller.

C. Legitimation of the closed-loop

The closed-loop formed by the recurrences (1) and (2) and the selection of sensing parameters (6) governs the evolution of the belief distribution of the parameter. Under this evolution, the cost function is a lower bound of the BMSE conditional to previous measurements $\mathbf{x}^{(k)} := \{x_1, \dots, x_k\}$ [13], [14], [29].

Proposition 1 (Properties of the closed-loop). The following relations hold for the closed-loop system formed by the Processor updates (1) and (2), and the Controller selection (6).

(i) *The motion and measurement updates satisfy*

$$p_k^-(\boldsymbol{\theta}_k) = p(\boldsymbol{\theta}_k | \mathbf{x}^{(k-1)}, \mathbf{g}^{(k)}) \quad (7a)$$

$$p_k^+(\boldsymbol{\theta}_k) = p(\boldsymbol{\theta}_k | \mathbf{x}^{(k)}, \mathbf{g}^{(k)}) \quad (7b)$$

$$c = \frac{1}{p(\mathbf{x}_k | \mathbf{x}^{(k-1)}, \mathbf{g}^{(k)})}, \quad (7c)$$

i.e., $p_k^+(\boldsymbol{\theta}_k)$ is the posterior belief at step k conditioned to all measurements $\mathbf{x}^{(k)}$ and sensing parameters $\mathbf{g}^{(k)}$.

(ii) *The WWB in the cost function (5) satisfies the inequality*

$$\begin{aligned} & \text{WWB}(\mathbf{H}; p(\mathbf{x}_k | \boldsymbol{\theta}_k, \mathbf{g}) p_k^-(\boldsymbol{\theta}_k)) \\ & \preceq \text{BMSE}(\hat{\boldsymbol{\theta}}_k, p(\mathbf{x}_k, \boldsymbol{\theta}_k | \mathbf{x}^{(k-1)}, \mathbf{g}^{(k-1)}, \mathbf{g})), \end{aligned}$$

where $\hat{\boldsymbol{\theta}}_k$ is any estimator based on $\mathbf{x}^{(k)}, \mathbf{g}^{(k-1)}, \mathbf{g}$. Similarly for the corresponding inequality taking trace $_{\rho}$ on both sides.

This result is proved in Appendix D. Relations (7) are what we would expect without selection of sensing parameters using previous measurements. Next we derive the WWB for a frequency estimation model based on array measurements.

III. STATISTICAL MODEL FOR MULTI-DIMENSIONAL FREQUENCY ESTIMATION FOR RANDOM INITIAL PHASE

In this section we derive the statistical performance bound based on the WWB for a family of array processing models under Gaussian and independent uniform priors. This metric can be used both for adaptation of transmission variables and for optimal design of constrained sparse arrays and sampling schemes (cf. [33]).

A. Observation model for spatio-temporal sampling

Here we present an observation model for array processing tasks that include direction of arrival (DoA) and Doppler estimation of a single source, and also MIMO schemes such as TDM MIMO.

Consider the following data model for an observation \mathbf{x} according to a sensing scheme depicted in Fig. 2,

$$\mathbf{x} = \mathbf{a}(\boldsymbol{\theta})\sqrt{\gamma} + \mathbf{n} \in \mathbb{C}^N, \quad (8)$$

where $\boldsymbol{\theta} := (u_1, \dots, u_{q-1}, \varphi)^T \in \mathbb{R}^q$ is the vector of unknown parameters, $\mathbf{n} \sim \mathcal{N}_{\mathbb{C}}(\mathbf{0}, \mathbf{I}_N)$ is standard complex Gaussian noise, and γ is the (single element) SNR, which is assumed known or estimated beforehand. Furthermore $\mathbf{a}(\boldsymbol{\theta})$ denotes the *spatio-temporal steering vector* for one source with frequencies u_j and initial phase φ , defined as

$$\mathbf{a}(\boldsymbol{\theta}) := e^{i\mathbf{D}\boldsymbol{\theta}} = e^{i\sum_j \mathbf{d}_j u_j} e^{i\varphi} \in \mathbb{C}^N, \quad (9)$$

which depends on the $q-1$ *sampling vectors* $\mathbf{d}_j \in \mathbb{R}^N$, which we combine, for convenience, to form the *sampling matrix*,

$$\mathbf{D} := (\mathbf{d}_1, \dots, \mathbf{d}_{q-1}, \mathbf{1}_N) \in \mathbb{R}^{N \times q}. \quad (10)$$

The sampling matrix $\mathbf{D} \equiv \mathbf{D}(\mathbf{g})$ can be parametrized by a sensing parameter \mathbf{g} that can be designed or adapted, and which we omit in this section. We refer to the generic parameter $\mathbf{u} = (u_1, \dots, u_{q-1})$ as *frequency vector*, whereas φ is called *initial phase* or *phase*.

This data model can be applied to the estimation of several quantities for one source, including DoA or Doppler estimation, where \mathbf{d}_1 refers to antenna positions or pulse times; joint azimuth-elevation estimation with 3-dimensional arrays [30, eq. (38)], where $\mathbf{d}_1, \mathbf{d}_2, \mathbf{d}_3$, are the coordinates of the antenna locations in some basis and $\boldsymbol{\theta}$ are the electronic angles; and range-Doppler-azimuth estimation [34] in automotive applications after a Fourier transform in the fast-time domain for each Tx and Rx pair and each pulse.

Next we show an example of application to the problem of TDM MIMO array processing for joint DoA-Doppler estimation [35]. This is a general template that we use in Section V-D for adaptive selection of antenna elements in the scenario of DoA estimation.

B. TDM MIMO DoA-Doppler estimation

Adaptive sampling for DoA-Doppler estimation can involve the activation of receivers and transmitter activation sequences. Consider N_{Rx} receivers in a linear array at positions $\mathbf{d}^{\text{Rx}} \in \mathbb{R}^{N_{\text{Rx}}}$ that collect the echoes from a total of N_{P} pulses transmitted by a subset of a total of N_{Tx} transmitters available, allowing repetitions, located at positions $\mathbf{d}^{\text{Tx}} \in \mathbb{R}^{N_{\text{Tx}}}$. The pulses are sent one after the other at time instances $\mathbf{t}^{\text{P}} \in \mathbb{R}^{N_{\text{P}}}$. The transmission variables to be optimized are (i) the specific *subset and order of transmitter activations*, codified by the matrix $\mathbf{G}^{\text{Tx}} \in \{0, 1\}^{N_{\text{P}} \times N_{\text{Tx}}}$ (where $\mathbf{1}_{N_{\text{P}}} = \mathbf{G}^{\text{Tx}} \mathbf{1}_{N_{\text{Tx}}}$); (ii) the *subset of N_{R} receivers* whose signals are processed, codified by, $\mathbf{G}^{\text{Rx}} \in \{0, 1\}^{N_{\text{R}} \times N_{\text{Rx}}}$; and (iii) possibly the carrier frequency. A model for the observation of a single target with DoA u , Doppler frequency $\omega = 4\pi v_r/\lambda$, and complex amplitude $s = |s|e^{i\varphi}$, is given by [35, eq. (4),(5)]

$$\mathbf{x} = \mathbf{b}(u, v_r, \varphi)|s| + \mathbf{n}, \quad (11)$$

where the spatio-temporal steering vector for TDM MIMO,

$$\mathbf{b}(u, v_r, \varphi) := e^{i\frac{1}{\lambda}(\mathbf{d}^{\text{V}}u + \mathbf{t}^{\text{V}}v_r)} e^{i\varphi},$$

can be written as in (9) in terms of the positions of the *active* virtual elements, i.e., pairs Tx, Rx, and the pulse times,

$$\begin{aligned} \mathbf{d}^{\text{V}} &:= \mathbf{G}^{\text{Tx}} \mathbf{d}^{\text{Tx}} \otimes \mathbf{1}_{N_{\text{R}}} + \mathbf{1}_{N_{\text{P}}} \otimes \mathbf{G}^{\text{Rx}} \mathbf{d}^{\text{Rx}} \\ \mathbf{t}^{\text{V}} &:= \mathbf{t}^{\text{P}} \otimes \mathbf{1}_{N_{\text{R}}}, \end{aligned}$$

(units of $\frac{1}{2\pi}$ for \mathbf{d}^{V} and $\frac{1}{4\pi}$ for \mathbf{t}^{V}) yielding the sampling matrix

$$\mathbf{D}(\mathbf{g}) = \frac{1}{\lambda}(\mathbf{d}^{\text{V}}, \mathbf{t}^{\text{V}}, \lambda \mathbf{1}_{N_{\text{P}}N_{\text{R}}}) \in \mathbb{R}^{N_{\text{P}}N_{\text{R}} \times 3}.$$

This fits into our general model (8) by identifying $\boldsymbol{\theta} = (u, v_r, \varphi)$ as parameters to be estimated, $\gamma = \frac{|s|^2}{\sigma^2}$ as SNR, $\mathbf{d}_1 = \frac{\mathbf{d}^{\text{V}}}{\lambda}$ as virtual array positions, and $\mathbf{d}_2 = \frac{\mathbf{t}^{\text{V}}}{\lambda}$ as virtual pulse times.

In the next section we describe the construction of the WWB for the model (9), (10) that includes the above scenarios.

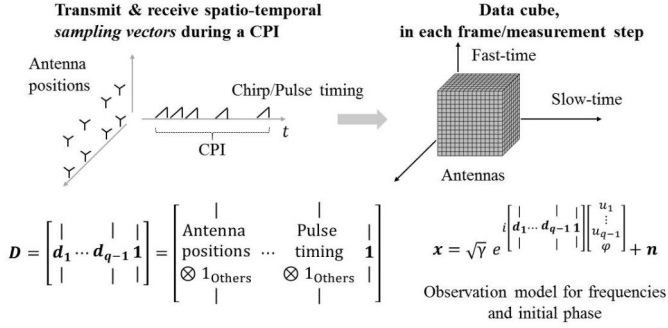


Fig. 2. Design of sensing parameters in spatial and temporal domains during a coherent processing interval (CPI), or frame, with random initial phase. The antenna positions and pulse timing can be nonuniform and sparse and can be selected or scaled between frames using the proposed Bayesian adaptive framework.

C. Random-phase WWB for array processing

Here we derive the WWB for the data model introduced in (8) both for Gaussian and independent uniform belief distributions on the frequency parameters. The calculation is similar to the general formulation in [30], but employs a different class of test points.

Performing the calculations outlined in the Appendix A for the choice of test point $\mathbf{h} = (h_{u_1}, \dots, h_{u_{q-1}}, h_\varphi)^T \in \mathbb{R}^{q \times 1}$, we obtain

$$\mathbf{WWB}(\mathbf{h}) = \frac{1}{Q} \mathbf{h} \mathbf{h}^T \in \mathbb{C}^{q \times q} \quad (12a)$$

$$Q = 2 \frac{\eta(\mathbf{h}, \mathbf{h}) - \eta(\mathbf{h}, -\mathbf{h})}{\eta(\mathbf{h}, \mathbf{0})^2} \quad (12b)$$

$$\eta(\mathbf{v}, \tilde{\mathbf{v}}) = \dot{\eta}(\mathbf{v}, \tilde{\mathbf{v}}) \xi(\mathbf{v}, \tilde{\mathbf{v}}) \quad (12c)$$

where the integral over observations $\dot{\eta} \equiv \dot{\eta}_\theta$ according to (27) is

$$\dot{\eta}(\mathbf{v}, \tilde{\mathbf{v}}) = \exp\left(-\frac{\gamma}{2} (N - \text{Re}\{\mathbf{1}_N^T e^{i\mathbf{D}(\tilde{\mathbf{v}}-\mathbf{v})}\})\right), \quad (13)$$

and the following integral over parameters remains to be determined after the choice of prior distribution,

$$\xi(\mathbf{v}, \tilde{\mathbf{v}}) := \int_{\Theta} p(\theta) \sqrt{\frac{p(\theta + \mathbf{v}) p(\theta + \tilde{\mathbf{v}})}{p(\theta)^2}} d\theta. \quad (14)$$

Analytic expressions for this integral are given in the Appendix B in the cases of Gaussian (33) and independent uniform (29) priors.

Remark 2 (Choice of test point matrix). *The computation of the WWB (22) requires to select a test point matrix \mathbf{H} . In [19, sec. 4.4.1.4], it is suggested to use test point matrices with at least as many columns M as rows q (i.e. number of random parameters in the model). While still being valid lower bounds, the WWB matrices that arise from test points with $M < q$ are by construction rank-deficient and therefore suboptimally suited to produce tight bounds to a presumably full-rank BMSE matrix. For the sake of simplicity in terms of derivation and computational time, we nonetheless select the test point matrix to comprise only one column and perform global optimization to find the tightest bound in this class.*

Remark 3 (Factorization of integrals). *Note that the factorization of $\eta = \dot{\eta} \cdot \xi$ in (12c) (cf. equation (26) in the Appendix) into the product of an integral over observations and an integral over parameters is due to the fact that, for this choice of model and parameters, the function $\dot{\eta}$ is independent of θ . Unfortunately, this is not true if e.g. the SNR γ is included into the set of random parameters θ or in the case of several targets. The consequence of the latter is an increase in computation time.*

Combining the expressions in (12), the optimization problem (5) can be written as

$$\mathcal{C} = \sup_{\mathbf{h} \in \mathcal{H}_\Theta} \text{trace}_\rho \mathbf{WWB}(\mathbf{h}) \quad (15)$$

for \mathbf{h} in the domain (cf. (25) in the Appendix)

$$\mathcal{H}_\Theta := \{\mathbf{h} \in \mathbb{R}^{q \times 1} : \Theta \cap (\Theta + \mathbf{h}) \neq \emptyset\}. \quad (16)$$

Note that this set depends on the prior belief through its support, $\Theta := \text{supp}(p(\theta)) = \{\theta \in \mathbb{R} : p(\theta) > 0\}$.

Remark 4 (Symmetry of WWB and \mathcal{H}_Θ). *A sufficient condition for the symmetry $\mathbf{WWB}(\mathbf{h}) = \mathbf{WWB}(-\mathbf{h})$ results from the corresponding symmetries $(\mathbf{v}, \tilde{\mathbf{v}}) \rightarrow (-\mathbf{v}, -\tilde{\mathbf{v}})$ for $\dot{\eta}$, which holds in general in view of (13), and also for ξ , which depends on the specific prior distribution. Since $\mathbf{h} \in \mathcal{H}_\Theta \iff -\mathbf{h} \in \mathcal{H}_\Theta$ by definition of \mathcal{H}_Θ in (16), this symmetry implies that we can neglect those test points of \mathcal{H}_Θ which are on one side of an arbitrarily chosen hyperplane through $\mathbf{0} \in \mathcal{H}_\Theta$ when solving the optimization problem (15). We thus choose to restrict the optimization to test points with positive phase component $\mathbf{h}_\varphi \geq 0$.*

For both uniform and Gaussian priors, the integral over priors ξ and thus the corresponding WWB (31), (34) depend only on the variance of the prior, and is independent of its mean.

The dependence on the prior only through the variance makes it convenient to numerically characterize the controller based on the corresponding WWB cost function for observation models in low-dimensional estimation and for low-dimensional sensing parameters. We study the controller output based on inputs given by distributions with this property for an array scaling task in the following section.

IV. ANALYSIS OF RANDOM-PHASE WWB FOR SCALING OF SAMPLING PERIOD

Here we analyze the WWB constructed in Section III for a model of frequency estimation in one dimension plus an extra dimension for the initial phase. We compare them with the corresponding bounds assuming a known initial phase in the decision problem of selecting the optimal scaling of the array. In particular, we characterize the controller choices numerically using a look-up table that can be used for real-time computation and also interpret the choices, specially the added robustness of considering the initial phase unknown.

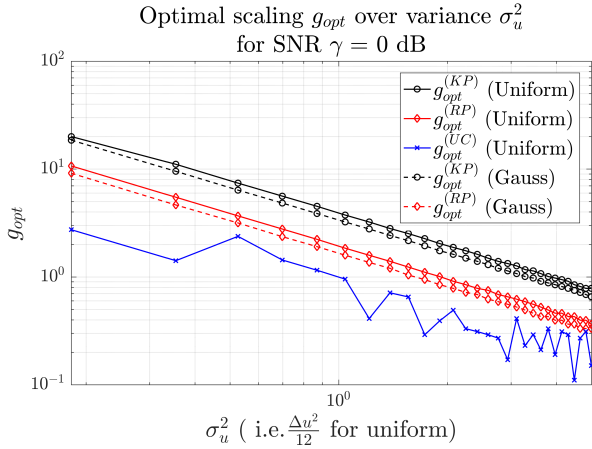


Fig. 3. Optimal scaling versus variance σ_u^2 of Gaussian and uniform priors. The optimal choices according to the Random-Phase WWB are depicted in red, the choices for the Known-Phase WWB [30, Eq. (57)] in black, and for the unconditional WWB [30, Eq. (56)] in blue.

A. Observation model for array scaling

We investigate the following estimation problem as a special case of model (8): Consider a sampling vector $\mathbf{d} \in \mathbb{R}^N$ that can be scaled by a factor $g_k \in \mathbb{R}_+$, that we wish to adapt at each measurement step $k = 1, 2, \dots$, according to the data model

$$\mathbf{x}_k = e^{ig_k \mathbf{d} u} e^{i\varphi_k} \sqrt{\gamma} + \mathbf{n}_k. \quad (17)$$

We recall that the Gaussian noise realizations $\mathbf{n}_k \sim \mathcal{N}_{\mathbb{C}}(0, \mathbf{I}_N)$ and the uniform random initial phases $\varphi_k \sim \mathcal{U}([-\pi, \pi])$ are assumed independent from each other and between time steps.

Regarding applications, the sampling vector and the frequency parameter in model (17) can have various interpretations. For instance, the scaling parameter can be the (inverse) wavelength λ of the carrier frequency in narrow-band DoA estimation, or the PRI for a train of pulses in Doppler estimation (after the range bin is determined). For adaptation steps on a time scale exceeding the coherency interval of the radar, the prescribed randomization of the initial phase is necessary. It is worth noting that even though these applications can be cast into the mathematical shape of model (17), it is necessary to reflect on how changing the scaling affects other radar properties in the context of the broader estimation task (e.g. changing the PRF affects range ambiguities). On the other hand, the more general array processing model (8) allows to consider these broader scenarios.

B. Characterization of controller for uniform array scaling

Here we analyze the controller choices based on optimization of the WWB cost function (15) for uniform and Gaussian priors, respectively given by expressions (34) and (31) in Section III-C. To this end, we visualize the dependence of the optimal scaling on prior variance and SNR value and compare with the results obtained from related statistical performance bounds.

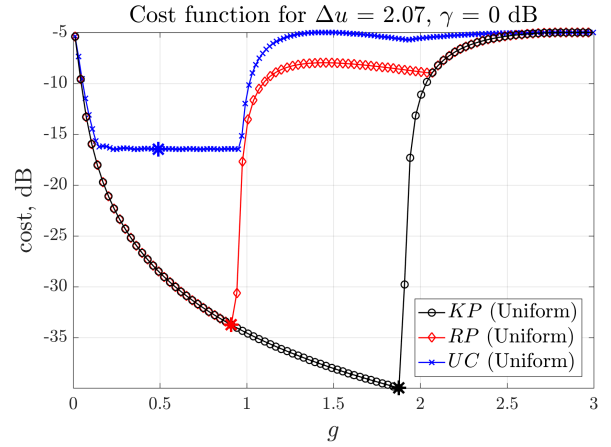


Fig. 4. Cost function $\mathcal{C}(g)$ for all three models. The unconditional model optimal scaling is harder to determine precisely for the unconditional model due to the slight variations in the cost function ‘basin’ and the optimal value is smaller and thus more conservative.

The scaling choices are computed for a uniform array of $N = 12$ elements with positions $\mathbf{d} = \pi(1, \dots, N) - \frac{N+1}{2}$ (naturally, other arrays are possible). The array’s center of mass is at the origin, i.e. $\hat{\mathbf{d}} = \frac{1}{N} \sum_n \mathbf{d}_n = 0$. We denote the optimal scaling choice according to the presented random-phase (RP) WWB in (31) and (34), as $g_{opt}^{(RP)} \equiv g_{opt}^{(RP)}(\sigma_u^2)$. Those depend only on the variance σ_u^2 of the Gaussian or uniform belief distribution, which indicates the certainty we have on the parameter u . For comparison, we discuss also the optimal scaling choices according to the WWBs for two slightly different models: the scalings referred to as $g_{opt}^{(KP)}$ are found from a *known-phase* (KP) model which assumes the phase φ as known (based on [30, Eq. (57)]), while the scalings referred to as $g_{opt}^{(UC)}$ correspond to an *unconditional* (UC) model with Gaussian amplitude based on [30, eq. (56)]. Details on the latter are provided in the Appendix C.

We focus on two aspects of the scaling selection, (i) the dependence on variance and SNR, and (ii) the sensitivity of the WWB with respect to variations of the optimal scaling.

a) *Dependencies of RP and KP models:* Regarding the dependence on variance (or Field-of-View length), consider Fig. 3 that shows the scaling selections for the RP model with uniform and Gaussian priors (red). As we expect, the more uncertainty we have about u (i.e. σ_u^2 large), the smaller the optimal array scaling g to avoid aliasing, and vice-versa, the more certainty about u (i.e. σ_u^2 small), the larger the scaling, to trade off ambiguity suppression with accuracy. The difference between Gaussian and uniform priors of same variance is comparatively insignificant. We observe that in this *high SNR scenario* with $\gamma = 0$ dB, the choices based on the KP WWB (black) are roughly twice the value as compared to the random-phase model, $g_{opt}^{(KP)} \approx 2g_{opt}^{(RP)}$. Further inspection (not shown here), reveals that this relationship holds for SNR values approximately above $\gamma = -1.5$ dB. For lower SNR values, we find that the optimal scalings according to the random and known-phase models coincide $g_{opt}^{(KP)} \approx g_{opt}^{(RP)}$.

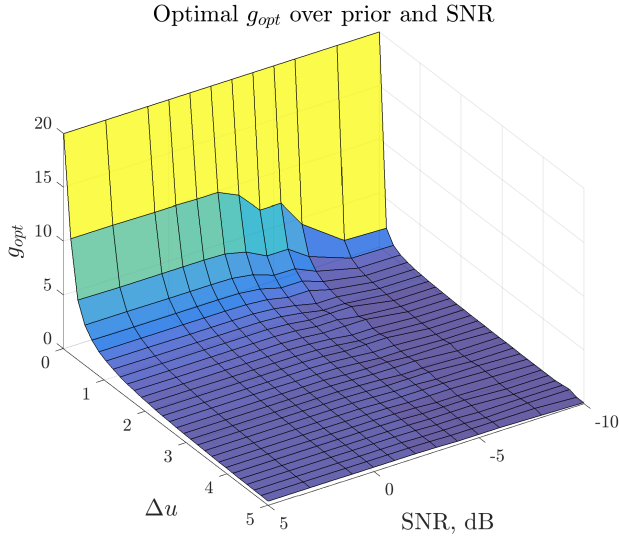


Fig. 5. Optimal scaling according to random-phase WWB versus SNR γ and support length Δu of uniform prior.

Remark 5 (Dependence of KP WWB on coordinate origin). *The known-phase WWB depends on the coordinate origin chosen to define the sampling vector \mathbf{d} , which in these visualizations is taken as the array center of mass. This makes it harder to analyze this WWB model and also argues against using it. This dependence also occurs for the Cramér-Rao bound (CRB) where the Fisher information matrix satisfies $\mathbf{FIM} = 2\gamma g^2 \|\mathbf{d}\|^2$ for the known-phase model, while for the random-phase model $\mathbf{FIM} = 2\gamma g^2 \|\mathbf{d} - \hat{\mathbf{d}}_{1N}\|^2$.*

b) *Dependencies of UC model:* The unconditional model considers a signal with random amplitude $s \sim \mathcal{N}_{\mathbb{C}}(0, \gamma')$ (cf. Appendix C) yielding a notion of SNR γ' with a different interpretation. The deterministic SNR notion γ of the other models obey an exponential distribution $\gamma \sim \text{Exp}(\gamma')$ under this model, such that, even though $\mathbb{E}[\gamma] = \gamma'$, a given value of γ' emphasizes low SNR values according to the previous notion. The optimal scaling $g_{opt}^{(UC)}$ (blue) in Fig. 3 (for $\gamma' = 0$ dB) is thus more conservative compared to the other models for high SNR. The unsteady behavior of the curve for the unconditional model can be understood in view of Fig. 4, which shows the cost function plotted over scalings. We observe that the unconditional model exhibits an almost flat 'basin' of low values with only slight oscillation in which the optimal scaling lies for this model. It is thus likely that the scaling in the optimization grid with the lowest cost function value is found in a neighboring peak of the analytical optimum. At low SNR, the respective scalings of the other two models (not shown here) are smaller than $g_{opt}^{(UC)}$. In summary, the optimal scaling does not depend very strongly on the SNR γ' for the unconditional model and is generally more conservative.

c) *Sensitivity of RP model:* With regards to the sensitivity of the RP WWB with respect to scaling, consider Figure 6 depicting the optimal choices for the case of uniform priors at both high and low SNR, including the value of the RP WWB

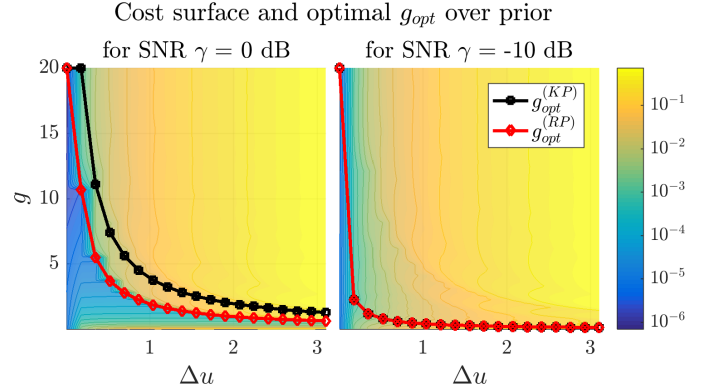


Fig. 6. Color code: random-phase (RP) WWB with uniform prior for each pair $(\Delta u, g)$. The red curve shows the optimal scaling for each Δu (i.e. minimum of RP WWB along each vertical line) at the given SNR. The black curve shows the corresponding scaling choice according to the known-phase WWB. For high SNR (left), we observe the latter yields consistently larger scalings. For low SNR (right), the choices of the known-phase WWB, which depend on the convention for the choice of coordinate origin, are the same as for the random-phase WWB.

cost (in color code) for each pair $(\Delta u, g)$. It is noteworthy, from a sensitivity perspective, the change of the RP WWB with respect to scaling choice. We observe that for high SNR (cf. left plot in Fig. 6), the optimal scaling according to the RP WWB $g_{opt}^{(RP)}$ (red), is only slightly smaller than scalings which abruptly exhibit significantly higher cost values, whereas for low SNR (cf. right plot of Fig. 6), the optimal scalings are not so close to such a *threshold*. This is relevant because for high SNR the optimal choices for the alternative metric of known-phase WWB $g_{opt}^{(KP)}$ (black) are slightly bigger and thus in the region of higher cost from the perspective of the RP WWB. This phenomenon is studied in the next section, where we show using the array factor that the RP WWB captures the notion of aliasing differently than the KP WWB.

C. Ambiguity function for optimal choices of known-phase and random-phase WWB for array scaling

Here we interpret the behavior of the RP WWB and the KP WWB calculated in the previous section in terms of the array factor for the same model of frequency estimation (17) as a function of array scaling. The array factor or ambiguity function with respect to the sampling vector (or array) \mathbf{d} is given by

$$\begin{aligned} B(u, u+h) &:= \frac{\langle e^{igdu}, e^{igd(u+h)} \rangle}{\|e^{igdu}\| \|e^{igd(u+h)}\|} \\ &= \frac{\langle \mathbf{1}_N, e^{igdh} \rangle}{N} = \frac{1}{N} \sum_{n=1}^N e^{igd_n h} \equiv B(h). \end{aligned} \quad (18)$$

This quantity appears in the WWB through the function η in (13). It can be interpreted in several ways: (i) Cosine distance or ambiguity function between signals e^{igdu} ; (ii) The discrete-time Fourier transform (DTFT), or projection, of a signal e^{igdu} into the frequency-shifted signal $e^{igd(u+h)}$. Figs. 7 and 8 depict the array factor of the optimal arrays for the RP and KP models, respectively, for a specific Field-of-View length Δu for two SNR values, $\gamma = 0$, regarded here

as *high*, and $\gamma = -10$, regarded as *low*. We make the following observations:

(i) For *high* SNR, the random-phase WWB favors the largest scaling which places the first grating lobe (i.e. smallest $h_1 > 0$ with $|B(h)| = 1$) right outside of Δu as measured from the main lobe (c.f. Fig. 7). This choice maximizes the accuracy (since larger apertures correspond to thinner mainlobes) while avoiding aliasing even for the extreme case of the parameter value being in the extremes of the prior belief distribution. This choice explains the sensitivity phenomenon displayed in Figs. 4 and 6 (left) where the cost function shows a dramatic increase for *bigger* scalings. A lesson from this regarding the application of the RP WWB for adaptive scaling is the following: if the prior is given by a uniform approximation of the filter's empirical density output, then the support length Δu needs to be chosen *conservatively*, at least in the case of *high* SNR.

(ii) For *low* SNR, the behavior is governed by the sidelobes (c.f. Fig. 8). In the context of Fig. 6 (right), we note that the optimal scaling is in a region of relatively small slope or change of the RP WWB. It is noteworthy that for *low* SNR below approximately -1.5 dB the KP WWB and RP WWB yield the same choice.

(iii) The KP WWB can identify only aliasing problems for test points that satisfy $\text{Re}\{B(h)\} = 1$. Their location depends on the convention for the array's center of mass \hat{d} . For a uniform array, the array factor is $B(h) = \frac{1}{N} e^{igh\hat{d}} \frac{\sin(N\frac{\pi gh}{2})}{\sin(\frac{\pi gh}{2})}$. Choosing the array's center of mass as coordinate origin (i.e. $\hat{d} = 0$), we find that every other of the grating lobes at $h_k = \frac{2k}{g}$ is a minimum for $\text{Re}\{B(h)\}$ if the number of observations N is even, and not a maximum as for $|B(h)|$. This is especially the case for the first grating lobe h_1 and thus the controller based on the known-phase WWB chooses, for fixed Δu , a scaling *twice as large than it should*. (In the case of the uniform array, we could choose an offset $\hat{d} = \pm \frac{\pi}{2}$ to detect the grating lobe of $\text{Re}\{B(h)\}$, but in general such an offset depends on the array.)

V. ADAPTIVE ARRAY SCALING AND CHANNEL SELECTION FOR FREQUENCY ESTIMATION

Here we apply the adaptive sensing framework of Section II using the WWB metric derived in Section III to the problem of frequency estimation in two scenarios: (i) adaptation of array *scaling*, and (ii) antenna selection. In the first case, the parameter optimized is 1-dimensional and we can use the numerical characterization in Section IV. In the second case, the parameter optimized is discrete, with as many elements as groups of antennas that can be active, and we use a neural network to fit the optimal test point evaluation of the WWB. First we define the Bayesian updates and their particle filter implementation, and then we simulate the closed-loop between the filter and the controller in both scenarios.

Array factor of optimal array for $\Delta u = 2.07$, $\gamma = 0$ dB
 $g_{opt}^{(RP)}(\Delta u, \gamma) = 0.91$

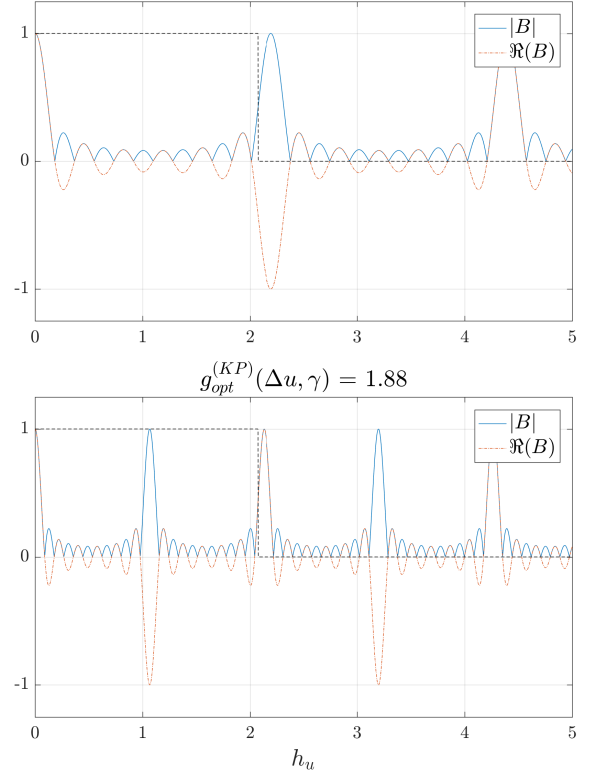


Fig. 7. Array factor (18) of optimal array according to the WWB for random-phase and known-phase models for *high* SNR. The *alternating symmetry* between the absolute value and the real part only appears when the coordinate origin is the center of mass. The optimal scaling according to RP WWB seems to depend on $B(h)$ through the absolute value (which is coordinate origin invariant), in contrast with the optimal scaling for the KP WWB that depends on the real part and thus depends on the coordinate origin.

Array factor of optimal array for $\Delta u = 2.07$, $\gamma = -10$ dB
 $g_{opt}^{(RP)}(\Delta u, \gamma) = g_{opt}^{(KP)}(\Delta u, \gamma) = 0.2$

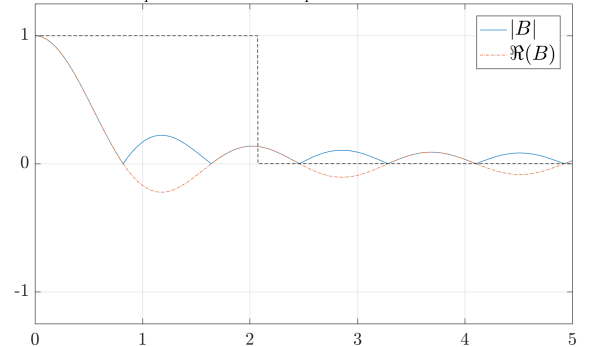


Fig. 8. Array factor (18) of optimal array according to the WWB for random-phase and known-phase models. At *low* SNR, the optimal scaling is the same for both models.

A. Bayesian measurement and motion updates

A characterization of the Bayesian filter requires to define the measurement and the motion updates. The likelihood function, $p(\mathbf{x}|\boldsymbol{\theta}, g)$ for $\boldsymbol{\theta} = (u, \varphi)^T \in \mathbb{R}^2$, required in the measurement update for model (17), obeys the general Gaussian model in (8) and is straightforward. The transition model between measurement steps is as follows. The frequency parameter of interest u is assumed, in this example, constant ($u_k = u, \forall k$) along the execution of the algorithm $k = 1, 2, \dots$, and the initial belief distribution is assumed uniform in the interval $[a, b]$. Naturally, other motion models can be implemented by the particle filter. The initial phase φ however, undergoes a transition that is crucial for our observation model: after each measurement step it is reinitialized at random, to capture the fact that no information is available due to incoherent measurements. Formally, the initial belief $p_0^+(\boldsymbol{\theta}_0)$ is uniform on the Cartesian product $[a, b] \times [-\pi, \pi]$, and the state evolution is modeled by

$$\boldsymbol{\theta}_k = \begin{pmatrix} u_{k-1} \\ 0 \end{pmatrix} + \begin{pmatrix} 0 \\ m_\varphi \end{pmatrix} \text{ with } m_\varphi \sim \mathcal{U}([-\pi, \pi]). \quad (19)$$

This yields transition probabilities independent of the scaling g_k , i.e.

$$p(\boldsymbol{\theta}_k|\boldsymbol{\theta}_{k-1}) = \delta_{u_{k-1}}(u_k) \frac{1}{2\pi} \chi_{[-\pi, \pi]}(\varphi_k).$$

The measurement and motion updates are implemented using a particle filter, described next.

B. Particle filter implementation

We employ a particle filter $\{\mathbf{p}_\theta, \mathbf{w}\}$ (see e.g. [20]), comprising N_P particles $\mathbf{p}_\theta = \{\boldsymbol{\theta}^i = (u^i, \varphi^i)^T\}_{i=1}^{N_P} \in \mathbb{R}^{q \times N_P}$ and weights $\mathbf{w} \in \mathbb{R}^{N_P \times 1}$ to represent, at each step $k \geq 1$, the belief distribution of $\boldsymbol{\theta}_k = (u_k, \varphi_k)^T \in \mathbb{R}^2$. The particle filter is initialized with particles drawn from $p_0^+(\boldsymbol{\theta}_0) := p_0(\boldsymbol{\theta}_0)$, i.e. uniformly at random from $[a, b] \times [-\pi, \pi]$, and with equal weights $\mathbf{w} = \frac{1}{N_P} \mathbf{1}_{N_P}$. The motion update required to obtain p_k^- can be realized with the particle filter by applying the target dynamics (19) independently to each particle. The measurement update is performed by resampling all particles at each step according to the weights given by the likelihood function $w_i = p(\mathbf{x}|\boldsymbol{\theta}^i, \mathbf{g})$ with the residual resampling method [36]; after the resampling the weights are reset to $\mathbf{w} = \frac{1}{N_P} \mathbf{1}_{N_P}$.

C. Simulation of adaptive array scaling

Here we compare in simulations the performance of the closed-loop between the Bayesian filter and the controllers described in Section IV-B in the sequential frequency estimation task (17). The resulting adaptive strategies are compared with a fixed scaling, a linearly increasing scaling, and a random scaling.

The metric used to evaluate the estimation quality of the policies is the average of squared-errors over N_T independent trials or executions of the algorithm at a given step k , where

the ground truth u_0 is drawn randomly according to the initial belief $p_0(\boldsymbol{\theta}_0)$ at the beginning of each trial,

$$\text{MSE}(\hat{u}_k) := \frac{1}{N_T} \sum_{n=1}^{N_T} ((\hat{u}_k)_n - (u_k)_n)^2, \quad (20)$$

and \hat{u}_k is the conditional mean estimator at the k -th step, $\hat{u}_k = \bar{\mathbf{p}}_{u_k} = \mathbf{p}_{u_k} \mathbf{w}$. Further simulation specifications are the following. The target SNR is fixed to $\gamma = -5$ dB and assumed known by the controller. To relax this condition a further dimension can be added to the particle filter and then the conditional mean estimate, or a conservative guess, can be used to evaluate the WWB. The sampling vector $\mathbf{d} \in \mathbb{R}^N$ consists of $N = 12$ uniformly spaced elements. We employ a particle filter with $N_P = 10^4$ particles to represent the joint belief distribution of the frequency parameter u and phase φ . The functional dependence of the optimal scaling $g = g(\Delta u, \gamma)$ for the WWB policies has been computed beforehand on a sufficiently fine grid (Fig. 5). The decision time of the controller is thus made negligible and it is suited for real-time applications. This computation speed is particularly beneficial to analyze the performance in simulations because we find that on the order of 10^4 trials are required to obtain reproducible results for the empirical mean squared error (MSE) defined in (20).

For the adaptive array scaling estimation task (17), using as objective function (15), in principle the prior can be approximated by the empirical density of the particles. However, computing the parameter integral via (14) for an arbitrary empirical density is expensive due to the large number of particles required for a good representation. For this reason, we approximate the belief distribution represented by the particles $(\mathbf{p}_\theta, \mathbf{w})$ by a uniform or Gaussian distribution of judiciously chosen variance, e.g., in terms of the empirical variance

$$\hat{\sigma}_u^2 = (\mathbf{p}_u - \bar{\mathbf{p}}_u \mathbf{1}_{N_P})^T \text{diag}(\mathbf{w}) (\mathbf{p}_u - \bar{\mathbf{p}}_u \mathbf{1}_{N_P}). \quad (21)$$

We have observed that the estimation quality of the adaptive sensing policies based on Gaussian and uniform approximations of the empirical density given by the particles can benefit from choosing a larger (i.e., more conservative) variance for the controller input, $\sigma_u^2 = \delta \cdot \hat{\sigma}_u^2$, i.e., multiplying by a factor the variance of the particles in (21). The choice of $\delta \geq 1$ that works well seems to depend on the SNR: For *high* SNR, the resulting policies benefit from bigger (more conservative) values. This can be explained based on the abrupt increase of cost reported in Fig. 6 (left), which reflects the fact that at high SNR there is a possibility of abruptly introducing aliasing in the field of view. For *low* SNR, as in the simulation with $\gamma = -5$ dB, choosing equal variances for the empirical and approximate distribution (i.e. $\delta = 1$) worked fine. This again can be due to the smaller sensitivity of the scaling with respect to the variance at low SNR as shown in Fig. 6 (right) wherein the cost is dominated by sidelobes and not by grating lobes.

Fig. 9 shows one realization of scaling choices for each of the strategies, while Fig. 10 shows the empirical MSE for 10^5 trials of each of the strategies, confirming the benefit of adaptation strategies over *ad hoc* policies without feedback. For the adaptive policies, we observe the influence of approximating

the empirical density of the particles by a Gaussian or uniform prior, which can have a bigger impact than the SNR modeling choice that distinguishes the RP and UC WWB.

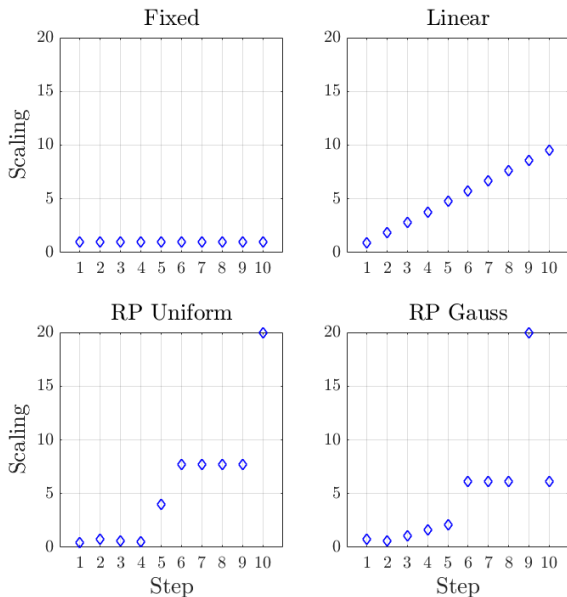


Fig. 9. Array scaling over measurement steps for one trial. Top: fixed choice and linearly increasing scaling. Bottom: our adaptive algorithms based on the RP WWB where the *priors* are given by the output of the particle filter approximated using uniform or Gaussian densities.

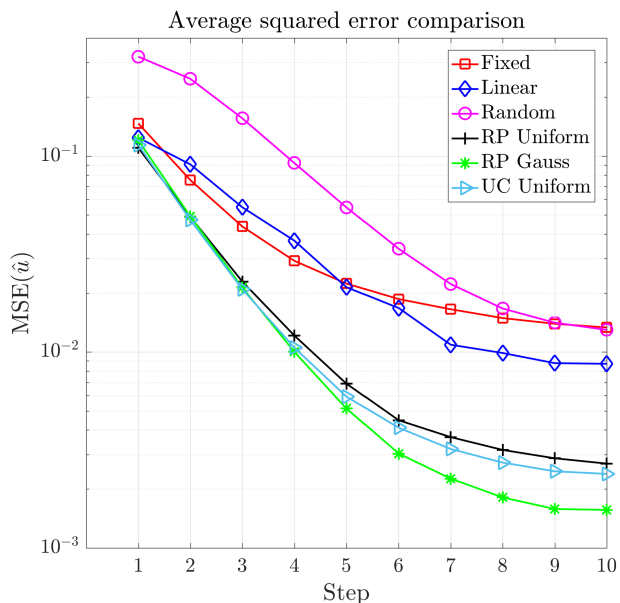


Fig. 10. Comparison of MSE at each step over 10^5 independent trials of each policy for SNR $\gamma = -5$ dB. Note that a high number of trials is necessary for this metric to converge because each choice of sensing parameters depends on the filtered belief distribution from the previous step and thus on the unique history of previous choices.

We find it interesting to compare, in addition to the average $MSE(\hat{u}_k)$, also the histogram of the squared errors at each step, cf. Fig. 11. It can be seen that the linear scaling strategy

often produces estimates equally exact as the adaptive strategy, but is more prone to outliers. Conversely, the fixed scaling, which is more conservative, is equally well suited to avoid outliers as the adaptive strategy, but in the prevailing part of trials its estimates are less accurate.

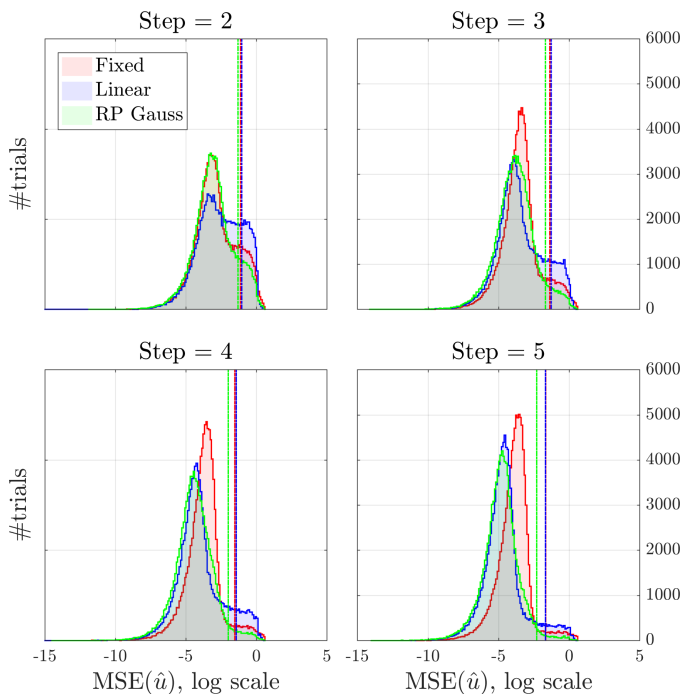


Fig. 11. Histogram of errors at given steps of the trial of the algorithm for each policy. The vertical lines represent the MSE over all trials at the given step. Note that at the beginning of each trial the ground truth is sampled randomly and therefore this metric resembles the empirical BMSE.

D. Simulation of adaptive channel selection

Here we simulate the controller performance for DoA estimation in TDM MIMO (11) assuming that Doppler is known and equal to 0. The controller needs to determine at each step the subset of transmitters and receivers that are active [15] [26].

In contrast with the case of array or sampling scaling, where the sensing parameter is one-dimensional and can be computed off-line, stored in a look-up table and interpreted visually, the adaptation of antenna selection presents a number of discrete choices that grows exponentially with the number of available antennas. This has motivated us to train a neural network to predict the values of the evaluation of the tightest WWB over test points in (5), cf. Fig. 1.

We have trained a fully connected neural network to approximate the KP WWB used in our previous work [26]. The concept is similar for the newly presented RP WWB. The input data comprises the antenna choices and the variance of the prior distribution, and the output is the optimal KP WWB (5). The choice of antennas is formatted using 1-hot encoding of the virtual array elements that are active for a scenario where the available Tx and Rx elements are placed in a uniform grid $0.9\{1, \dots, 8\}$ in units of half-wavelength, and Tx 1 and Rx

1 are fixed. That is, at each step the controller chooses one transmitter and one receiver out of 7 available.

For training, we have used the *Tensorflow* library for *Python*. For this small problem, the neural network is allowed to overfit the training data because we have computed the WWB in a sufficiently fine grid of variance values. The problem remains for the future to show the application of the closed-loop Bayesian adaptive framework in Fig. 1 to scenarios where the neural network learns to abstract relevant array properties based on limited training data.

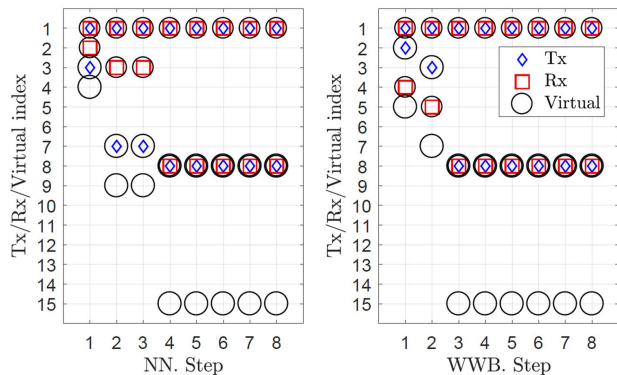


Fig. 12. Channel selection at each measurement step for one trial of the policies defined by a fixed choice, the KP WWB, and a neural network that approximates the KP WWB. The prior distribution is assumed Gaussian with variance equal to the variance of the distribution given by the particle filter. (Overlapping virtual elements are represented with concentric circles.)

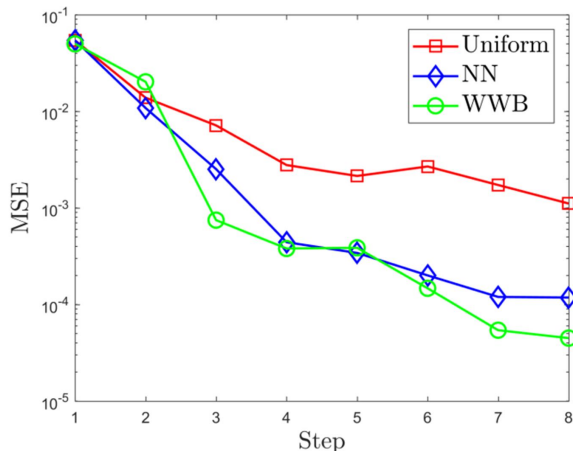


Fig. 13. Comparison of MSE for policies using the KP WWB [26], [30], the associated neural network approximation, and the uniform MIMO array with Tx $\{1, 3\}$ and Rx $\{1, 2\}$. The MSE is obtained at each step averaging over 300 realizations of the measurement.

In Fig. 12 we show that the antenna choices in a typical execution of the neural network resemble the ones of the exact WWB, and Fig. 13 shows that the performance is similar. From a computation standpoint, this example shows the practical side of the adaptive framework in Fig. 1 based on previous work of the authors [26].

VI. CONCLUSIONS

We have studied frequency estimation tasks for radar arrays in the context of a Bayesian setting where adaptation of sampling vectors based on the WWB prediction of estimation error is shown to be feasible for real-time implementations, at least at the software level, and provides a significant improvement of accuracy. From the ambiguity function standpoint, we have discussed the impact of incorporating knowledge of the phase or lack thereof in the model of the WWB, as this modeling choice affects the characterization of aliasing.

We have derived the Weiss-Weinstein bound for a generic multi-dimensional frequency estimation model for a single source with random initial phase, which can be efficiently implemented for uniform and Gaussian priors, and stated the optimization problem rigorously to obtain optimal sensing parameters. We have shown the applicability in two scenarios of 1D sequential frequency estimation, adapting, respectively, the scaling of sampling vector or PRF, e.g., for Doppler estimation, and antenna selection for DoA estimation. In the first case we have characterized the optimal controller choices of scaling parameter in terms of prior variance and SNR. By storing the values in a look-up table, we can achieve real-time computation. Analogously, in the case of antenna selection for DoA estimation, we have shown that a neural net trained off-line can overfit the predictions of the WWB for a given SNR, suggesting that the evaluation of the optimal WWB is feasible for real-time implementations.

Future work needs to address the bottleneck of the computational cost of the WWB for empirical densities, e.g., given by a particle filter. This may be overcome with neural networks trained off-line using as input not the variance but a higher-detail representation of the densities. Through this means, one might obtain well adjusted sensing choices for a larger class of belief distributions than currently possible with Gaussian or uniform approximations of the empirical densities. We also envision applications of this framework to scenarios like channel selection in TDM MIMO for joint DoA and Doppler estimation, and PRF adaptation for ground moving target indication (GMTI) with colored noise. Quantitative guarantees on the benefits of adaptation are also an open problem, particularly to complement the need of numerical analysis that requires a large number of Monte Carlo realizations in multi-dimensional problems to extract conclusions about the average behavior of the closed-loop.

VII. ACKNOWLEDGMENTS

The authors would like to thank the German Ministry of Defense, particularly the WTD 81, for supporting this work. We also thank Prof. Joseph Tabrikian for helpful discussions on the topic during the German-Israeli exchange program TA44 and the anonymous reviewers that helped us improve the quality of the paper.

REFERENCES

- [1] S. Haykin. *Cognitive Dynamic Systems: Perception-Action Cycle, Radar and Radio*. Cambridge University Press, 2012.

- [2] F. Gini, A. De Maio, and L. K. Patton. *Waveform design and diversity for advanced radar systems*. The Institution of Engineering and Technology (IET), 2012.
- [3] M. Wicks, E. Mokole, S. Blunt, and R. Schneible. *Principles of waveform diversity and design*. The Institution of Engineering and Technology (IET), 2011.
- [4] S. D. Blunt and E. L. Mokole. Overview of radar waveform diversity. *IEEE Aerospace and Electronic Systems Magazine*, 31(11):2–42, November 2016.
- [5] R. A. Romero, J. Bae, and N. A. Goodman. Theory and application of SNR and mutual information matched illumination waveforms. *IEEE Transactions on Aerospace and Electronic Systems*, 47(2):912–927, April 2011.
- [6] N. A. Goodman, P. R. Venkata, and M. A. Neifeld. Adaptive waveform design and sequential hypothesis testing for target recognition with active sensors. *IEEE Journal of Selected Topics in Signal Processing*, 1(1):105–113, June 2007.
- [7] A. Charlish, K. Woodbridge, and H. Griffiths. Phased array radar resource management using continuous double auction. *IEEE Transactions on Aerospace and Electronic Systems*, 51(3):2212–2224, 2015.
- [8] Z. Ding. A survey of radar resource management algorithms. In *Canadian Conf. on Electrical and Computer Engineering (CCECE)*, pages 1559–1564, 2008.
- [9] A. Aubry, A. De Maio, M. Piezzo, M. M. Naghsh, M. Soltanalian, and P. Stoica. Cognitive radar waveform design for spectral coexistence in signal-dependent interference. In *IEEE Radar Conference*, pages 0474–0478, May 2014.
- [10] P. Stinco, M. S. Greco, and F. Gini. Spectrum sensing and sharing for cognitive radars. *IET Radar, Sonar Navigation*, 10(3):595–602, 2016.
- [11] J. R. Guerci, R. M. Guerci, M. Ranagaswamy, J. S. Bergin, and M. C. Wicks. CoFAR: Cognitive fully adaptive radar. In *2014 IEEE Radar Conference*, pages 0984–0989, May 2014.
- [12] F. Smits, A. Huizing, W. van Rossum, and P. Hiemstra. A cognitive radar network: Architecture and application to multiplatform radar management. In *European Radar Conference*, pages 312–315, Oct 2008.
- [13] W. Huleihel, J. Tabrikian, and R. Shavit. Optimal adaptive waveform design for cognitive MIMO radar. *IEEE Transactions on Signal Processing*, 61(20):5075–5089, 2013.
- [14] O. Isaacs, J. Tabrikian, and I. Bilik. Cognitive antenna selection for optimal source localization. In *IEEE 6th International Workshop on Computational Advances in Multi-Sensor Adaptive Processing (CAMSAP)*, pages 341–344, Dec 2015.
- [15] J. Tabrikian, O. Isaacs, and I. Bilik. Cognitive antenna selection for DOA estimation in automotive radar. In *IEEE Radar Conference*, pages 1–5, May 2016.
- [16] P. Chavali and A. Nehorai. Scheduling and power allocation in a cognitive radar network for multiple-target tracking. *IEEE Transactions on Signal Processing*, 60(2):715–729, 2012.
- [17] S. Haykin. Cognitive Radar: A way of the future. *IEEE Signal Processing Magazine*, 23(1):30–40, Jan 2006.
- [18] K. L. Bell, C. J. Baker, G. E. Smith, J. T. Johnson, and M. Rangaswamy. Cognitive Radar framework for target detection and tracking. *IEEE Journal of Selected Topics in Signal Processing*, 9(8):1427–1439, Dec 2015.
- [19] H. L. Van Trees and K. L. Bell. *Detection, Estimation, and Modulation Theory*. Wiley, 2 edition, 2013.
- [20] M. S. Arulampalam, S. Maskell, N. Gordon, and T. Clapp. A tutorial on particle filters for online nonlinear/non-gaussian Bayesian tracking. *IEEE Transactions on Signal Processing*, 50(2):174–188, Feb 2002.
- [21] A. Weiss and E. Weinstein. A lower bound on the mean-square error in random parameter estimation. *IEEE Trans. on Information Theory*, 31(5):680–682, Sep 1985.
- [22] A. Renaux, P. Forster, P. Larzabal, C. D. Richmond, and A. Nehorai. A fresh look at the Bayesian bounds of the Weiss-Weinstein family. *IEEE Transactions on Signal Processing*, 56(11):5334–5352, 2008.
- [23] D. Khan and K. L. Bell. Analysis of DOA estimation performance of sparse linear arrays using the Ziv-Zakai bound. In *IEEE Radar Conference*, pages 746–751, May 2010.
- [24] N. D. Tran, A. Renaux, R. Boyer, S. Marcos, and P. Larzabal. Weiss-Weinstein bound for MIMO radar with colocated linear arrays for SNR threshold prediction. *Signal Processing*, 92(5):1353–1358, 2012.
- [25] K. L. Bell, J. T. Johnson, G. E. Smith, C. J. Baker, and M. Rangaswamy. Cognitive Radar for target tracking using a Software Defined Radar system. In *IEEE Radar Conference*, pages 1394–1399, May 2015.
- [26] D. Mateos-Núñez, M. A. González-Huici, R. Simoni, and S. Brüggewirth. Adaptive channel selection for DOA estimation in MIMO radar. In *IEEE International Workshop on Computational Advances in Multi-Sensor Adaptive Processing (CAMSAP)*, Dec 2017.
- [27] I. Rapoport and Y. Oshman. Weiss-Weinstein lower bounds for Markovian systems. Part 1: Theory. *IEEE Transactions on Signal Processing*, 55(5):2016–2030, May 2007.
- [28] F. Xaver, P. Gerstoft, G. Matz, and C. F. Mecklenbräuer. Analytic sequential Weiss-Weinstein bounds. *IEEE Transactions on Signal Processing*, 61(20):5049–5062, Oct 2013.
- [29] N. Sharaga, J. Tabrikian, and H. Messer. Optimal cognitive beamforming for target tracking in MIMO radar/sonar. *IEEE Journal of Selected Topics in Signal Processing*, 9(8):1440–1450, Dec 2015.
- [30] D. Thang Vu, A. Renaux, R. Boyer, and S. Marcos. Some results on the Weiss-Weinstein bound for conditional and unconditional signal models in array processing. *Signal Processing*, 95:126–148, 2014.
- [31] S. Herbert, J. R. Hopgood, and B. Mulgrew. MMSE Adaptive waveform design for active sensing with applications to MIMO radar. *IEEE Transactions on Signal Processing*, 66(5):1361–1373, March 2018.
- [32] S. Kirkpatrick, C. D. Gelatt, and M. P. Vecchi. Optimization by simulated annealing. *Science*, 220(4598):671–680, 1983.
- [33] M. A. González-Huici, D. Mateos-Núñez, C. Greiff, and R. Simoni. Constrained optimal design of automotive radar arrays using the Weiss-Weinstein bound. In *International Conference on Microwaves for Intelligent Mobility (ICMIM)*, 2018. Can be found in [arXiv:1804.08608v1](https://arxiv.org/abs/1804.08608v1).
- [34] F. Engels, P. Heidenreich, A. M. Zoubir, F. K. Jondral, and M. Wintermantel. Advances in Automotive Radar: A framework on computationally efficient high-resolution frequency estimation. *IEEE Signal Processing Magazine*, 34(2):36–46, March 2017.
- [35] K. Rambach, M. Vogel, and B. Yang. Optimal Time Division Multiplexing schemes for DOA estimation of a moving target using a colocated MIMO radar. In *IEEE International Symposium on Signal Processing and Information Technology*, pages 000108–000113, Dec 2014.
- [36] R. Douc and O. Cappé. Comparison of resampling schemes for particle filtering. In *Proceedings of the 4th International Symposium on Image and Signal Processing and Analysis*, pages 64–69, Sept 2005.
- [37] T. Kailath. The Divergence and Bhattacharyya distance measures in signal selection. *IEEE Trans. on Comm. Technology*, 15(1):52–60, February 1967.

APPENDIX

A. Background on the Weiss-Weinstein bound

For convenience of the reader, we include here the general expression of the WWB for Gaussian observations following [19] and [30]. These are the expressions that we explicitly evaluate in Section III-C for our array processing models with random initial phase in the case of uniform and Gaussian priors. The parametric family of Weiss-Weinstein bounds $\text{WWB}(\mathbf{H}) \in \mathbb{R}^{q \times q}$ for a data model comprising observations $\mathbf{x} \in \Omega \subseteq \mathbb{C}^N$ and random parameter vector $\boldsymbol{\theta} \in \mathbb{R}^q$ depends on their joint probability distribution $p(\mathbf{x}, \boldsymbol{\theta})$ and is defined by

$$\text{WWB}(\mathbf{H}) := \mathbf{H}\mathbf{Q}^{-1}\mathbf{H}^T, \quad (22)$$

where the elements of the matrix $\mathbf{Q} \in \mathbb{R}^{M \times M}$ are given by [30]

$$Q_{k,l} := \frac{\eta(\mathbf{h}_k, \mathbf{h}_l) + \eta(-\mathbf{h}_k, -\mathbf{h}_l) - \eta(\mathbf{h}_k, -\mathbf{h}_l) - \eta(-\mathbf{h}_k, \mathbf{h}_l)}{\eta(\mathbf{h}_k, \mathbf{0})\eta(\mathbf{0}, \mathbf{h}_l)}. \quad (23)$$

The real-valued function η is the expectation of scaled "likelihood ratios" $l(\mathbf{x}; \tilde{\boldsymbol{\theta}}, \boldsymbol{\theta}) := \frac{p(\mathbf{x}, \tilde{\boldsymbol{\theta}})}{p(\mathbf{x}, \boldsymbol{\theta})}$ given by

$$\eta(\mathbf{v}, \tilde{\mathbf{v}}) = \mathbb{E}_{p(\mathbf{x}, \boldsymbol{\theta})} [l^{\frac{1}{2}}(\mathbf{x}; \boldsymbol{\theta} + \mathbf{v}, \boldsymbol{\theta}) l^{\frac{1}{2}}(\mathbf{x}; \boldsymbol{\theta} + \tilde{\mathbf{v}}, \boldsymbol{\theta})]. \quad (24)$$

It is related to the *Bayesian Bhattacharyya coefficient* [28] and quantifies the overlap between the shifted densities on the support of the unshifted density. The matrix of test points has the shape $\mathbf{H} = (\mathbf{h}_1, \dots, \mathbf{h}_M) \in \mathbb{R}^{q \times M}$ for some $M \geq 1$, although $M \geq q$ is recommended in [19, seq. 4.4.1.4].

The domain of valid test points \mathcal{H}_Θ is restricted for practical purposes at least to matrices \mathbf{H} satisfying

$$\mathcal{H}_\Theta := \{\mathbf{H} \in \mathbb{R}^{q \times M} : \Theta \cap (\Theta + \mathbf{h}_m) \neq \emptyset, \forall m\} \quad (25)$$

where $\Theta := \text{supp}(p(\boldsymbol{\theta})) = \{\boldsymbol{\theta} \in \mathbb{R}^q : p(\boldsymbol{\theta}) > 0\}$ denotes the support of the prior. Note that if the intersection of supports in (25) was empty for one i , then $\eta(\mathbf{h}_i, \mathbf{0}) = 0$ and therefore \mathbf{Q}^{-1} cannot be computed since the i -th row/column of \mathbf{Q} is not defined.

In practice, the joint probability distribution is decomposed as $p(\mathbf{x}, \boldsymbol{\theta}) = p(\mathbf{x}|\boldsymbol{\theta})p(\boldsymbol{\theta})$, because the likelihood function $p(\mathbf{x}|\boldsymbol{\theta})$, denoting the probability of the observation \mathbf{x} given the parameter vector $\boldsymbol{\theta}$, and the prior probability distribution $p(\boldsymbol{\theta})$, can be modeled more naturally. With regard to equation (24), we find

$$\eta(\mathbf{v}, \tilde{\mathbf{v}}) = \int_{\Theta} \dot{\eta}_{\boldsymbol{\theta}}(\mathbf{v}, \tilde{\mathbf{v}}) p^{\frac{1}{2}}(\boldsymbol{\theta} + \mathbf{v}) p^{\frac{1}{2}}(\boldsymbol{\theta} + \tilde{\mathbf{v}}) d\boldsymbol{\theta}, \quad (26)$$

where $\dot{\eta}_{\boldsymbol{\theta}}(\mathbf{v}, \tilde{\mathbf{v}}) = \int_{\Omega} p^{\frac{1}{2}}(\mathbf{x}|\boldsymbol{\theta} + \mathbf{v}) p^{\frac{1}{2}}(\mathbf{x}|\boldsymbol{\theta} + \tilde{\mathbf{v}}) d\mathbf{x}$.

Up to this point the formulation of the WWB applies to general probability distributions of vector parameters and vector observations. Now we consider likelihood functions corresponding to Gaussian observation models parametrized by the mean, as for the *conditional model* described in [30], where $\mathbf{x} \sim \mathcal{N}_{\mathbb{C}}(\mathbf{a}(\boldsymbol{\theta}), \mathbf{R})$ with a known noise covariance matrix \mathbf{R} . The authors of [30, eq. (15)] offer the following analytic expression for the integration of likelihoods over observation space

$$\log \dot{\eta}_{\boldsymbol{\theta}}(\mathbf{v}, \tilde{\mathbf{v}}) = -\frac{1}{4} \|\mathbf{R}^{-1/2}(\mathbf{a}(\boldsymbol{\theta} + \mathbf{v}) - \mathbf{a}(\boldsymbol{\theta} + \tilde{\mathbf{v}}))\|^2 \quad (27)$$

which is obtained after using the parallelogram law to the terms that remain after a null addition trick to complete the Gaussian integral.

B. Integral ξ for uniform and Gaussian priors

Here we give explicit formulas for the WWB in (12) for Gaussian and uniform priors providing expressions for (14). These priors can be applied to design problems, such as array design, where the parameter of interest is assumed in a given interval or Field-of-View [33]. In this work, we use them in our Bayesian adaptive algorithm to approximate the outcome of the particle filter and accelerate the computations of the controller.

1) *Uniform belief distribution*: Consider a uniform belief distribution with support $\Theta \subset \mathbb{R}^q$ for the parameter of interest, $\boldsymbol{\theta} \sim \mathcal{U}(\Theta)$, i.e., $p(\boldsymbol{\theta}) = \frac{1}{|\Theta|} \chi_{\Theta}(\boldsymbol{\theta})$. We restrict our analysis to independent parameters. This implies a rectangular support

$$\Theta = (\boldsymbol{\mu}_{\mathbf{u}} + \times_j [-\frac{\Delta u_j}{2}, \frac{\Delta u_j}{2}]) \times [-\pi, \pi] =: [\boldsymbol{\alpha}, \boldsymbol{\beta}] \quad (28)$$

of volume $|\Theta| = 2\pi \prod_j \Delta u_j$ with edge lengths $\Delta \mathbf{u} \in \mathbb{R}^{q-1}$ and covariance $\boldsymbol{\Sigma}_{\mathbf{u}} = \text{diag}([\frac{\Delta u_j^2}{12}])$.

Using (28), the integral over priors ξ in (14) takes the form

$$\xi(\mathbf{v}, \tilde{\mathbf{v}}) = \frac{|\tilde{\Theta}(\mathbf{v}, \tilde{\mathbf{v}})|}{|\Theta|}, \quad (29)$$

where the volume $|\tilde{\Theta}(\mathbf{v}, \tilde{\mathbf{v}})|$ of the shifted-support intersection

$$\begin{aligned} \tilde{\Theta}(\mathbf{v}, \tilde{\mathbf{v}}) &:= \Theta \cap (\Theta - \mathbf{v}) \cap (\Theta - \tilde{\mathbf{v}}) \\ &= (\max(\boldsymbol{\alpha}, \boldsymbol{\alpha} - \mathbf{v}, \boldsymbol{\alpha} - \tilde{\mathbf{v}}), \min(\boldsymbol{\beta}, \boldsymbol{\beta} - \mathbf{v}, \boldsymbol{\beta} - \tilde{\mathbf{v}})) \end{aligned}$$

can be readily seen to be

$$\begin{aligned} |\tilde{\Theta}(\mathbf{v}, \tilde{\mathbf{v}})| &= \prod_j r([\boldsymbol{\beta} - \boldsymbol{\alpha} + \min(\mathbf{0}, -\mathbf{v}, -\tilde{\mathbf{v}}) - \max(\mathbf{0}, -\mathbf{v}, -\tilde{\mathbf{v}})]_j) \\ &= \prod_j r([\boldsymbol{\beta} - \boldsymbol{\alpha} - \frac{1}{2}(|\mathbf{v} - \tilde{\mathbf{v}}| + |\mathbf{v}| + |\tilde{\mathbf{v}}|)]_j) \end{aligned} \quad (30)$$

where $r(x) := \max(0, x)$ is the ramp function, i.e. the product $|\tilde{\Theta}(\mathbf{v}, \tilde{\mathbf{v}})|$ must be set to zero if one of the factors is negative. We thus find the expression

$$\text{WWB}(\mathbf{h}) = \frac{\mathbf{h}\mathbf{h}^T}{2|\Theta|} \frac{\dot{\eta}(\mathbf{h}, \mathbf{0})^2 |\tilde{\Theta}(\mathbf{h})|^2}{|\tilde{\Theta}(\mathbf{h})| - \dot{\eta}(\mathbf{h}, -\mathbf{h}) |\tilde{\Theta}(\mathbf{h}, -\mathbf{h})|} \quad (31)$$

with

$$\dot{\eta}(\mathbf{h}, \mathbf{0}) = \exp(-\frac{\gamma}{2}(N - \mathbf{1}_N^T e^{i\mathbf{D}\mathbf{h}})) \quad (32a)$$

$$\dot{\eta}(\mathbf{h}, -\mathbf{h}) = \exp(-\frac{\gamma}{2}(N - \mathbf{1}_N^T e^{i2\mathbf{D}\mathbf{h}})) \quad (32b)$$

$$|\tilde{\Theta}(\mathbf{h})| = (2\pi - |h_{\varphi}|) \prod_j (\Delta u_j - |h_{u_j}|)$$

$$|\tilde{\Theta}(\mathbf{h}, -\mathbf{h})| = \max(0, 2\pi - 2|h_{\varphi}|) \prod_j \max(0, \Delta u_j - 2|h_{u_j}|).$$

Depending on the shape of the support Θ , the function ξ can exhibit certain symmetries. For the case of our rectangular domain (28), we easily observe $\xi(\mathbf{v}, \tilde{\mathbf{v}}) = \xi(-\mathbf{v}, -\tilde{\mathbf{v}})$ from the representation in (30). As noticed in Remark 4, the optimization in (15) can be performed for $\mathbf{h} \in (\times_j [-\Delta u_j, \Delta u_j]) \times [0, 2\pi]$.

2) *Gaussian belief distribution*: Consider a Gaussian belief distribution for the frequency parameter $\mathbf{u} \sim \mathcal{N}_{\mathbb{R}}(\boldsymbol{\mu}_{\mathbf{u}}, \boldsymbol{\Sigma}_{\mathbf{u}})$, which is independent of the uniformly distributed phase φ , i.e.

$$p(\boldsymbol{\theta}) = p(\mathbf{u})p(\varphi)$$

$$p(\mathbf{u}) = \frac{1}{\sqrt{(2\pi)^{q-1} \det(\boldsymbol{\Sigma}_{\mathbf{u}})}} \exp(-\frac{1}{2} \|\mathbf{u} - \boldsymbol{\mu}_{\mathbf{u}}\|_{\boldsymbol{\Sigma}_{\mathbf{u}}^{-1}})$$

$$p(\varphi) = \frac{1}{2\pi} \chi_{[-\pi, \pi]}(\varphi).$$

Denoting $\Phi := [-\pi, \pi]$, the integral over priors ξ in (14) becomes

$$\xi(\mathbf{v}, \tilde{\mathbf{v}}) = \text{BC}(\mathbf{v}_{\mathbf{u}}, \tilde{\mathbf{v}}_{\mathbf{u}}) \cdot \frac{1}{2\pi} |\tilde{\Phi}(\mathbf{v}_{\varphi}, \tilde{\mathbf{v}}_{\varphi})| \quad (33)$$

$$\text{BC}(\mathbf{v}_{\mathbf{u}}, \tilde{\mathbf{v}}_{\mathbf{u}}) = \exp(-\frac{1}{8} \|\mathbf{v}_{\mathbf{u}} - \tilde{\mathbf{v}}_{\mathbf{u}}\|_{\boldsymbol{\Sigma}_{\mathbf{u}}^{-1}}^2)$$

$$|\tilde{\Phi}(\mathbf{v}_{\varphi}, \tilde{\mathbf{v}}_{\varphi})| = |\Phi \cap (\Phi - \mathbf{v}_{\varphi}) \cap (\Phi - \tilde{\mathbf{v}}_{\varphi})|$$

$$= \max(0, 2\pi - \frac{1}{2}(|\mathbf{v}_{\varphi} - \tilde{\mathbf{v}}_{\varphi}| + |\tilde{\mathbf{v}}_{\varphi}| + |\mathbf{v}_{\varphi}|))$$

where we used the expression for the Bhattacharyya coefficient for the case of two Gaussians with same variance but different means [37, eq. (61)]. (The derivation follows along the same

lines as the derivation of the expression for the complex Gaussian likelihood integral in (27).) We thus find the expression

$$\text{WWB}(\mathbf{h}) = \frac{\mathbf{h}\mathbf{h}^T \dot{\eta}(\mathbf{h}, \mathbf{0})^2 (\text{BC}(\mathbf{h}_u, \mathbf{0}) |\tilde{\Phi}(\mathbf{h}_\varphi)|)^2}{2(2\pi) |\tilde{\Phi}(\mathbf{h}_\varphi)| - \dot{\eta}(\mathbf{h}, -\mathbf{h}) \text{BC}(\mathbf{h}_u, -\mathbf{h}_u) |\tilde{\Phi}(\mathbf{h}_\varphi, -\mathbf{h}_\varphi)|} \quad (34)$$

with $\dot{\eta}$ as in (32a), (32b), and

$$\begin{aligned} |\tilde{\Phi}(\mathbf{h}_\varphi)| &= 2\pi - |\mathbf{h}_\varphi| \\ |\tilde{\Phi}(\mathbf{h}_\varphi, -\mathbf{h}_\varphi)| &= \max(0, 2\pi - 2|\mathbf{h}_\varphi|) \\ \text{BC}(\mathbf{h}_u, \mathbf{0}) &= \exp\left(-\frac{1}{8} \|\mathbf{h}_u\|_{\Sigma_u^{-1}}^2\right) \\ \text{BC}(\mathbf{h}_u, -\mathbf{h}_u) &= \exp\left(-\frac{1}{2} \|\mathbf{h}_u\|_{\Sigma_u^{-1}}^2\right). \end{aligned}$$

The optimization (15) is for $\mathbf{h} \in \mathbb{R}^{q-1} \times [0, 2\pi]$ since the symmetry $\xi(\mathbf{v}, \tilde{\mathbf{v}}) = \xi(-\mathbf{v}, -\tilde{\mathbf{v}})$ noticed in Remark 4 is evident from (33).

C. Background on the unconditional WWB

For convenience of the reader we include the unconditional WWB [30, eq. (56)]. It is based on the model $\mathbf{x} = \mathbf{a}(u)s + \mathbf{n} \in \mathbb{C}^N$, where \mathbf{n} is standard complex Gaussian noise, the steering vector is $\mathbf{a}(u) = e^{idu}$ and the complex amplitude $s \sim \mathcal{N}_{\mathbb{C}}(0, \gamma')$ is also a Gaussian random variable, i.e. $|s|^2 \sim \frac{\gamma'}{2} \chi_2^2 = \text{Exp}(\gamma')$ has an exponential distribution. Note that the notion of SNR according to the *KP* and *RP* models, denoted as γ , is related to γ' by $\mathbb{E}[|s|^2] = \mathbb{E}[\gamma] = \gamma'$. When the belief distribution on u is a uniform prior of length Δu , the corresponding WWB reads

$$\text{UWWB}(\mathbf{h}) = \frac{\mathbf{h}^2}{2\Delta u} \times \frac{(\Delta u - |\mathbf{h}|)^2 \left(1 + \frac{\kappa}{4} (N^2 - |1_N^T e^{idh}|^2)\right)^{-2}}{(\Delta u - |\mathbf{h}|) - \max(0, \Delta u - 2|\mathbf{h}|) \left(1 + \frac{\kappa}{4} (N^2 - |1_N^T e^{i2dh}|^2)\right)^{-1}} \quad (35)$$

where $\kappa = \frac{\gamma'^2}{N\gamma'+1}$. Inspiration for this formula came from eq. [30, eq. (56)], which is the special case for $\Delta u = 2$. The ramp function $r(x) = \max(0, x)$ is required when optimization is performed over $\mathcal{H}_\Theta = [-\Delta u, \Delta u]$. Due to the symmetry $h \rightarrow -h$, the optimization can be restricted to $[0, \Delta u]$.

D. Bound on BMSE conditioned to previous history

Here we prove Proposition 1. We restate part i) in the following Lemma where we spell out the assumed probability dependencies that hold for our observation and transition models.

Lemma 1 (Motion and measurement updates under sequence of sensing parameters). *Let the following assumptions be satisfied*

(i) *State independence of previous measurements, i.e.*

$$p(\boldsymbol{\theta}_k | \boldsymbol{\theta}_{k-1}, \mathbf{g}_k) = p(\boldsymbol{\theta}_k | \boldsymbol{\theta}_{k-1}, \mathbf{x}^{(k-1)}, \mathbf{g}^{(k)}) \quad (36)$$

(ii) *Conditional independence to next sensing parameter, i.e.*

$$p(\boldsymbol{\theta}_{k-1} | \mathbf{x}^{(k-1)}, \mathbf{g}^{(k-1)}) = p(\boldsymbol{\theta}_{k-1} | \mathbf{x}^{(k-1)}, \mathbf{g}^{(k)}).$$

(iii) \mathbf{x}_k is independent of $\mathbf{g}^{(k-1)}, \mathbf{x}^{(k-1)}$ given $\boldsymbol{\theta}_k$ and \mathbf{g}_k , i.e.,

$$p(\mathbf{x}_k | \boldsymbol{\theta}_k, \mathbf{g}_k) = p(\mathbf{x}_k | \boldsymbol{\theta}_k, \mathbf{x}^{(k-1)}, \mathbf{g}^{(k-1)}, \mathbf{g}_k). \quad (37)$$

Then the recurrences for the motion and measurement updates (1) and (2) satisfy (7).

Proof. We carry out the proof by complete induction. We can see the assertions to hold for $k = 0$ by definition of p_0^+ . Now suppose it is true for $k - 1$. To show (7a), we note that

$$\begin{aligned} & \int p(\boldsymbol{\theta}_k | \boldsymbol{\theta}_{k-1}, \mathbf{g}_k) p_{k-1}^+(\boldsymbol{\theta}_{k-1}) d\boldsymbol{\theta}_{k-1} \\ &= \int p(\boldsymbol{\theta}_k | \boldsymbol{\theta}_{k-1}, \mathbf{x}^{(k-1)}, \mathbf{g}^{(k)}) p(\boldsymbol{\theta}_{k-1} | \mathbf{x}^{(k-1)}, \mathbf{g}^{(k-1)}) d\boldsymbol{\theta}_{k-1} \\ &= \int p(\boldsymbol{\theta}_k, \boldsymbol{\theta}_{k-1} | \mathbf{x}^{(k-1)}, \mathbf{g}^{(k)}) d\boldsymbol{\theta}_{k-1} = p(\boldsymbol{\theta}_k | \mathbf{x}^{(k-1)}, \mathbf{g}^{(k)}). \end{aligned}$$

In the first step we use (i) and the hypotheses of induction for $p_{k-1}^+(\boldsymbol{\theta}_{k-1})$; afterwards we use assumption (ii) and standard properties of probabilities. To show (7b), we note that

$$\begin{aligned} p_k^+(\boldsymbol{\theta}_k) &= c p(\mathbf{x}_k | \boldsymbol{\theta}_k, \mathbf{g}_k) p(\boldsymbol{\theta}_k | \mathbf{x}^{(k-1)}, \mathbf{g}^{(k)}) \\ &= c p(\mathbf{x}_k | \boldsymbol{\theta}_k, \mathbf{x}^{(k-1)}, \mathbf{g}^{(k)}) p(\boldsymbol{\theta}_k | \mathbf{x}^{(k-1)}, \mathbf{g}^{(k)}) \\ &= \tilde{c} p(\boldsymbol{\theta}_k | \mathbf{x}_k, \mathbf{x}^{(k-1)}, \mathbf{g}^{(k)}) \end{aligned}$$

where in the 2nd step we have used assumption (iii), and in the last step we have used Bayes rule applied to the probability $\tilde{p}(\mathbf{x}_k | \boldsymbol{\theta}_k) := p(\mathbf{x}_k | \boldsymbol{\theta}_k, \mathbf{x}^{(k-1)}, \mathbf{g}^{(k)})$, resulting in $\tilde{c} = c \cdot p(\mathbf{x}_k | \mathbf{x}^{(k-1)}, \mathbf{g}^{(k)})$. Since the normalizing constant c is chosen so that p_k^+ is a probability density, it is $\tilde{c} = 1$, and we obtain the value for c in (7c). \square

Next we observe that the sensing parameters optimized according to (5) satisfy condition (ii) in Lemma 1.

Remark 6. *Consider the selection of sensing parameters according to (5) and (6). Then, for $k \geq 1$, it holds that*

$$p(\boldsymbol{\theta}_{k-1} | \mathbf{x}^{(k-1)}, \mathbf{g}^{(k-1)}) = p(\boldsymbol{\theta}_{k-1} | \mathbf{x}^{(k-1)}, \mathbf{g}^{(k)}),$$

where for $k = 1$ it is understood that $p(\boldsymbol{\theta}_0) = p(\boldsymbol{\theta}_0 | \mathbf{g}_1)$.

This follows from the fact that \mathbf{g}_k is computed in a deterministic manner in (6) from the previous observations $\mathbf{x}^{(k-1)}$ and sensing parameters $\mathbf{g}^{(k-1)}$ (requiring in addition only the initial belief $p(\boldsymbol{\theta}_0) = p_0(\boldsymbol{\theta}_0)$ and the transition and measurement models to carry out the recurrences (1) and (2)). As such, \mathbf{g}_k is independent of every other random variable conditioned to $\mathbf{x}^{(k-1)}$ and $\mathbf{g}^{(k-1)}$, and is in particular independent of $\boldsymbol{\theta}_{k-1}$.

Using the previous results we can provide the proof of Proposition 1. Proof of i) follows from Lemma 1.

Proof of ii) in Proposition 1. Follows using the identity in (7a) for $p_k^-(\boldsymbol{\theta}_k)$ (see Lemma 1) in inequality (4). Note that the assumptions (i) and (iii) of Lemma 1 are satisfied for the observation and transition models considered, and condition (ii) is verified in Remark 6. \square